SIMPLIFYING CHEMICAL KINETICS: TRAJECTORY-GENERATED LOW-DIMENSIONAL MANIFOLDS

by

S.B. Pope and U. Maas

FDA 93-11 November 1993

ABSTRACT

Our quantitative knowledge of combustion chemistry is embodied in detailed reaction mechanisms, which continue to advance in their scope and accuracy. In computations of combustion in complex flows (e.g. multidimensional laminar flows, turbulence simulations or turbulent combustion modelling) the computational cost of using a detailed reaction mechanism is excessive, and usually prohibitive. Consequently, there is motivation to develop computationally-simpler approximate methods based on detailed reaction mechanisms. In this paper, a new method (TGLDM) for the simplification of chemical kinetics is presented and demonstrated. A fundamental assumption in all simplification strategies—made explicit in manifold methods—is that the thermochemical compositions everywhere in a reactive flow lie close to a low-dimensional manifold in the high-dimensional composition space. In the TGLDM method, the low-dimensional manifold (of dimensional $d \geq 1$) $\mathcal{M}_d$ is formed by the reaction trajectories from a $(d-1)$-dimensional generator. For the simplest case of a 1D manifold for premixed combustion, $\mathcal{M}_1$ is just the reaction trajectory originating from the unburnt mixture composition. The method is developed here in the context of premixed combustion, and is demonstrated for a CO/H_2-air mixture. For the severe test case of a transient perfectly stirred reactor, it is shown that the 2D TGLDM method accurately describes the evolution of major and minor species.

INTRODUCTION

There are now many examples of laminar flame calculations based on the solution of conservations equations incorporating detailed reaction schemes (e.g. Smooke et al. [1], Warnatz [2]). These schemes may involve of order 50 species and 200 reactions. Consequently their use in complex flows is computationally expensive, and indeed the computational time required is often prohibitive. To perform computations of complex reactive flows, it is desirable, therefore, to have a simplified description of the chemistry, based on many fewer variables than the number of species. The reason to suppose that such a simplification is possible, is that reactive systems typically encountered in combustion contain many modes that relax on time scales much smaller than the flow time scales, and that therefore can be decoupled.

There has been much work in recent years on *reduced kinetic mechanisms* for different fuels (see e.g. refs. 3, 4, 5). Part of the reduction process is to make specific assumptions, such as partial equilibrium or steady-state. The approach presented here is somewhat different, in that it is a general methodology applicable to any fuel, and that specific assumptions are avoided—although certainly there are assumptions and approximations inherent in the method. Such general approaches have previously been attempted by Keck [6], Chen [7], Frenklach [8], and ourselves [9, 10]. The method considered here—*Trajectory-Generated Low-Dimensional Manifolds (TGLDM)*—is distinct from our earlier approach [9, 10]—*Intrinsic Low-Dimensional Manifolds (ILDM)*—although it shares the same motivation, and many of the same concepts. The two methods are contrasted in the discussion, below.

The TGLDM method is applicable to any single-phase reactive system; but, for simplicity of exposition, it is developed here in the context of premixed combustion. In the next section, the equations governing premixed combustion are presented from a geometric viewpoint. Then the basic concepts and issues in manifold methods are presented. These main issues are: the definition of the manifold; its parametrization; and the specification of a projection matrix. The specifics of the TGLDM method are then described, and test results are reported for both 1D and 2D manifolds. The test considered is a transient perfectly-stirred reaction (PSR) for a CO/H_2-air mixture. A "truncated projection"—designed to further reduce the computational cost of the method—is then described and tested. The paper closes with a discussion of various aspects of the TGLDM method.

FORMULATION

We consider the simplest case of constant-pressure premixed combustion (with the neglect of radiative heat loss, differential diffusion, and Lewis number effects). Consequently, the pressure p, the enthalpy h, and the elemental composition of the mixture are constant and uniform.

There are n_e elements and n_s species. At a given position $\mathbf{x}$ and time t, the mass fraction of species α is m_α, and the *specific mole number* of α is

$$\phi_\alpha = m_\alpha / M_{(\alpha)}, \tag{1}$$

where $M_{(\alpha)}$ is the molecular weight. Together with p and h, the n_s mole numbers ϕ_α completely define the thermochemical state of the fluid.

The *composition space* $\mathcal{C}$ is defined to be n_s-dimensional Euclidean space; and we introduce the set of orthonormal basis vectors $\mathbf{e}_\alpha$ $(\alpha = 1, 2, \ldots, n_s)$. Then the fluid composition is represented by the point $\boldsymbol{\phi} = \mathbf{e}_\alpha \phi_\alpha$ in composition space. (Summation is implied over repeated suffices, unless they are in parentheses.)

The *element vector* (for element β) is defined by

$$\boldsymbol{\mu}_\beta = \mathbf{e}_\alpha \mu_{\alpha\beta}, \tag{2}$$

where $\mu_{\alpha\beta}$ is the number of atoms of element β in a molecule of species α. Then the *specific element mole number* of element β is

$$\chi_\beta = \phi_\alpha \mu_{\alpha\beta} = \boldsymbol{\phi} \cdot \boldsymbol{\mu}_\beta. \tag{3}$$

This is simply the number of kg-moles of element β in a kg of mixture: and, for the premixed combustion considered, it is constant and uniform.

The *realizable region* $\mathcal{C}_R$ is defined to be the subset of composition space $\mathcal{C}$ corresponding to compositions that can occur. The two conditions that realizable compositions satisfy are that mass fractions are non-negative

$$\phi_\alpha \geq 0, \ \alpha = 1, 2, \ldots, n_s, \tag{4}$$

and that the specific element mole numbers equal their known constant values

$$\boldsymbol{\phi} \cdot \boldsymbol{\mu}_\beta = \chi_\beta, \ \beta = 1, 2, \ldots, n_e. \tag{5}$$

Together, these last two equations identify $\mathcal{C}_R$ as a convex $(n_s - n_e)$-dimensional polytope.

There are two distinguished points in $\mathcal{C}_R$. The first is the point corresponding to unburnt mixture (denoted by $\boldsymbol{\phi}^m$), the second is the point corresponding to equilibrium (denoted by $\boldsymbol{\phi}^e$).

For the given pressure and enthalpy, all thermochemical properties are known functions of $\boldsymbol{\phi}$. Equations of state give the temperature $T(\boldsymbol{\phi})$ and density $\rho(\boldsymbol{\phi})$, and the detailed reaction mechanism gives the reaction rate vector $\mathbf{S}(\boldsymbol{\phi})$, i.e. the rate of change of $\boldsymbol{\phi}$ due to reaction.

A central concept in the TGLDM method is that of a *reaction trajectory*, which is now defined. The equation

$$\frac{d}{dt}\boldsymbol{\phi}(t) = \mathbf{S}(\boldsymbol{\phi}(t)), \tag{6}$$

governs the evolution of a spatially-homogeneous composition field (which, because of homogeneity, is unaffected by convection and diffusion). Starting from the initial condition $\boldsymbol{\phi}(0) = \boldsymbol{\phi}^*$ (where $\boldsymbol{\phi}^*$ is any point in $\mathcal{C}_R$), the solution to Eq. (6) after time t is denoted by $\boldsymbol{\phi}^R(t, \boldsymbol{\phi}^*)$. The curve

$$\{\boldsymbol{\phi}^R(t, \boldsymbol{\phi}^*) : t \in [0, \infty)\} \tag{7}$$

is called the *reaction trajectory generated by* $\boldsymbol{\phi}^*$, and $\boldsymbol{\phi}^R(t, \boldsymbol{\phi}^*)$ gives its coordinates parametrized by time t. It is assumed that the reaction rate $\mathbf{S}$ is non-zero everywhere in $\mathcal{C}_R$ except at equilibrium, where it is of course zero. This, together with the fact that the Gibbs free energy decreases along the trajectory, ensures that as $t \to \infty$ all trajectories converge on the equilibrium point $\boldsymbol{\phi}^e$. In addition, the smoothness of $\mathbf{S}$ ensures that trajectories do not cross prior to their convergence on the equilibrium point.

At a given point $\mathbf{x}$ in an inhomogeneous premixed reactive flow, the composition $\boldsymbol{\phi}(t)$ evolves by

$$\frac{\partial \boldsymbol{\phi}(\mathbf{x}, t)}{\partial t} = \mathbf{S}(\boldsymbol{\phi}(\mathbf{x}, t)) + \mathbf{F}(\mathbf{x}, t), \tag{8}$$

where $\mathbf{F}(\mathbf{x}, t)$ denotes the effects of convection and molecular diffusion. It should be observed that, while the reaction rate $\mathbf{S}$ is a known function of the local composition, the effects of inhomogeneities embodied in $\mathbf{F}$ depend on the velocity and composition field in the neighborhood of $\mathbf{x}$. Hence, in the

present development, we regard $\mathbf{F}(\mathbf{x}, t)$ as an unknown perturbation (with no implied assumption that it is "small").

Examples and test results are given below for a CO/H_2-air mixture. In this there are 4 elements (C, O, H, N) and there are 13 species (H_2O, CO_2, N_2, O_2, H_2, CO, OH, H, O, HO_2, HCO, H_2O_2 and CH_2O), i.e. $n_e = 4$, $n_s = 13$. The initial mixture consists of CO, H_2, O_2 and N_2 in the mole ratios 24:18:21:97, at a temperature of 300K and a pressure of 1 bar. The reaction mechanism, consisting of 67 elementary reactions, is the same as that used by Maas & Pope [9].

BASIC CONCEPTS OF MANIFOLD METHODS

The fundamental assumption of manifold methods is that (at any point and time in the reactive flow) the composition $\boldsymbol{\phi}(\mathbf{x}, t)$—viewed as a point in the realizable composition space $\mathcal{C}_R$—is close to a low-dimensional attracting manifold, $\mathcal{M}$. For definiteness, we consider a two-dimensional manifold $\mathcal{M}$ in $\mathcal{C}_R$ parametrized by two variables u and v. The mapping from the *parameter space* $\mathcal{P}$ (i.e. a region of the $u-v$ plane) to the manifold is denoted by $\boldsymbol{\Phi}(u, v)$. That is, to every point (u, v) in the parameter space, there corresponds a realizable composition $\boldsymbol{\Phi}(u, v)$.

Restated, the fundamental assumption is that there is a manifold $\mathcal{M}$ (with coordinate $\boldsymbol{\Phi}(u, v)$) and there are parameter values $u(\mathbf{x}, t)$ and $v(\mathbf{x}, t)$ such that $\boldsymbol{\Phi}(u[\mathbf{x}, t],\ v[\mathbf{x}, t])$ provides an adequate approximation to $\boldsymbol{\phi}(\mathbf{x}, t)$. Consequently, the thermochemical state of the fluid at $(\mathbf{x}, t)$ is characterized by just two variables ($u(\mathbf{x}, t)$ and $v(\mathbf{x}, t)$); and the evolution of the composition field can be determined from the evolution equations for these two variables (deduced below), rather than from the n_s evolution equations for $\boldsymbol{\phi}$ (i.e. Eq. 8).

What is the basis for this fundamental assumption? What can cause the composition $\boldsymbol{\phi}$—which has a large number $(n_s - n_e)$ of degrees of freedom in $\mathcal{C}_R$—to be confined to a two-dimensional manifold? The validity of the assumption depends on the reaction rates $\mathbf{S}(\boldsymbol{\phi})$ and on the magnitude of the perturbations $\mathbf{F}$; a complete discussion is provided by Maas & Pope [9, 10]. Simply put, if all but two of the degrees of freedom in the reaction scheme

have time scales much smaller than that associated with $\mathbf{F}$, then a composition $\boldsymbol{\phi}(t)$ that is not on the manifold, will (due to reaction) very rapidly approach the manifold. In the end, the validity of the assumption, and the magnitude of the approximation involved must be determined empirically by tests such as those described below.

At a given point $\mathbf{x}$, we want to determine the time evolution of $u(t)$ and $v(t)$ such that $\boldsymbol{\Phi}(u(t), v(t))$ remains a good approximation to $\boldsymbol{\phi}(t)$. The rate of change of $\boldsymbol{\Phi}(u(t), v(t))$ is a vector in the tangent plane of the manifold: specifically

$$\frac{\partial \boldsymbol{\Phi}}{\partial t} = \boldsymbol{\Phi}_u \frac{\partial u}{\partial t} + \boldsymbol{\Phi}_v \frac{\partial v}{\partial t}, \tag{9}$$

where the tangent vectors are

$$\boldsymbol{\Phi}_u(u,v) = \frac{\partial \boldsymbol{\Phi}(u,v)}{\partial u} \quad \text{and} \quad \boldsymbol{\Phi}_v(u,v) = \frac{\partial \boldsymbol{\Phi}(u,v)}{\partial v}. \tag{10}$$

The rate of change of $\boldsymbol{\phi}(t)$ (i.e. $\dot{\boldsymbol{\phi}} = \mathbf{S} + \mathbf{F}$, see Eq. 8), on the other hand, is not constrained to lie in the tangent plane. Hence $\partial \boldsymbol{\Phi}/\partial t$ and $\partial \boldsymbol{\phi}/\partial t$ cannot be equated. But the evolution of $\boldsymbol{\Phi}$ can be made to approximate that of $\boldsymbol{\phi}$ by equating $\partial \boldsymbol{\Phi}/\partial t$ to a *projection* of $\partial \boldsymbol{\phi}/\partial t$ onto the tangent plane. With $\mathbf{P}(u,v)$ denoting a specified $(n_s \times n_s)$ projection matrix, the above reasoning leads to the equation

$$\boldsymbol{\Phi}_u \frac{\partial u}{\partial t} + \boldsymbol{\Phi}_v \frac{\partial v}{\partial t} = \mathbf{P} \cdot (\mathbf{S} + \mathbf{F}). \tag{11}$$

Then it is a matter of algebra to show that u evolves by

$$\frac{\partial u}{\partial t} = \dot{u}_s + \dot{u}_F = \mathbf{P}^u \cdot (\mathbf{S} + \mathbf{F}), \tag{12}$$

where $\dot{u}_s = \mathbf{P}^u \cdot \mathbf{S}$, $\dot{u}_F = \mathbf{P}^u \cdot \mathbf{F}$, and the projection vector $\mathbf{P}^u(u,v)$ is

$$\mathbf{P}^u = \left\{ (\boldsymbol{\Phi}_v \cdot \boldsymbol{\Phi}_v)\, \boldsymbol{\Phi}_u \cdot \mathbf{P} - (\boldsymbol{\Phi}_u \cdot \boldsymbol{\Phi}_v)\, \boldsymbol{\Phi}_v \cdot \mathbf{P} \right\} / \left\{ (\boldsymbol{\Phi}_u \cdot \boldsymbol{\Phi}_u)\, (\boldsymbol{\Phi}_v \cdot \boldsymbol{\Phi}_v) - (\boldsymbol{\Phi}_u \cdot \boldsymbol{\Phi}_v)^2 \right\}. \tag{13}$$

And similar equations express $\partial v/\partial t$ in terms of a second projection vector $\mathbf{P}^v$.

From the above development, it may be seen that the principal issues in manifold methods are

i) the definition and determination of the manifold $\mathcal{M}$, including its dimensionality.

ii) the determination of a suitable parametrization of $\mathcal{M}$ and the identification of the parameter space $\mathcal{P}$.

iii) the specification of the projection matrix $\mathbf{P}$.

Different manifold methods correspond to different treatments of these three issues. Indeed (as discussed by Maas & Pope [9, 10]) most reduced kinetics schemes can be viewed as manifold methods, and hence the implied specification of $\mathcal{M}$, $\mathbf{P}$ and the parametrization can be deduced.

The computational implementation of manifold methods consists of two stages. In the first (pre-processing) stage (which needs to be performed only once for a given mixture) the following quantities are tabulated as functions of u and v: $\boldsymbol{\Phi}$, $\dot{u}_s \equiv \mathbf{P}^u \cdot \mathbf{S}$, $\dot{v}_s \equiv \mathbf{P}^v \cdot \mathbf{S}$, $\mathbf{P}^u$, $\mathbf{P}^v$ as well as any other thermochemical variable required in the flow calculation or needed for output (e.g. temperature and density). Then, in the second stage, during the flow calculation, $u(\mathbf{x}, t)$ and $v(\mathbf{x}, t)$ are taken as the independent thermochemical variables. At any $(\mathbf{x}, t)$, all thermochemical properties are determined by interpolation from the tables (e.g. $\boldsymbol{\Phi}(u, v)$). Hence the perturbation $\mathbf{F}$ due to convection and diffusion can be evaluated, and the dot product $\dot{u}_F = \mathbf{P}^u \cdot \mathbf{F}$ formed. The equation for u ($\partial u/\partial t = \dot{u}_s + \dot{u}_F$) can then be advanced in time by, and similarly for v.

TRAJECTORY-GENERATED MANIFOLDS

The ILDM method developed by Maas & Pope [9, 10] is in some senses optimal: the manifolds generated are "most attracting," and the projection matrix is appropriately based on the eigenvectors of $\partial S_\alpha/\partial \phi_\beta$. But the implementation of the method is somewhat involved, largely because the method *per se* does not provide a parametrization of the manifold.

In the *Trajectory-Generated Low-Dimensional Manifold* (TGLDM) method now presented, the emphasis is on simplicity. The manifolds are defined in terms of reaction trajectories, and hence can be constructed simply by integrating Eq. (6). The way in which the manifolds are defined introduces a natural parametrization, with the parameter space $\mathcal{P}$ being extremely simple

(e.g. the unit circle or square in 2D). The perpendicular projection is used, so that the projection vectors can be simply determined from the manifold, without further appeal to the kinetics.

An important property of trajectory-generated manifolds is that the reaction-rate vector $\mathbf{S}$ is in the tangent plane. Hence the projection does not affect $\mathbf{S}$ (i.e. $\mathbf{P} \cdot \mathbf{S} = \mathbf{S}$), and so the choice of projection affects only the treatment of the perturbation term $\mathbf{P} \cdot \mathbf{F}$.

We now define the one-dimensional and two-dimensional manifolds for the TGLDM method.

The one-dimensional manifold $\mathcal{M}_1$ is simply the reaction trajectory generated by the mixing point, $\boldsymbol{\phi}^m$, i.e.

$$\mathcal{M}_1 = \left\{ \boldsymbol{\phi}^R(t, \boldsymbol{\phi}^m) : t \in [0, \infty) \right\}. \tag{14}$$

This is obtained by integrating the Eq. (6) (i.e. $\dot{\boldsymbol{\phi}} = \mathbf{S}(\boldsymbol{\phi})$) from the initial condition $\boldsymbol{\phi}(0) = \boldsymbol{\phi}^m$, corresponding to unburnt mixture.

The solution of Eq. (6) yields $\boldsymbol{\phi}^R(t, \boldsymbol{\phi}^m)$, i.e. the manifold parametrized by time t. It is more convenient to use the normalized arclength along the trajectory as the parameter: hence we define u to be the arclength along the trajectory from $\boldsymbol{\phi}^m$, normalized by the total arclength. Consequently $u = 0$ corresponds to unburnt mixture, $u = 1$ corresponds to equilibrium, and so u can be interpreted as a reaction progress variable. And with $\boldsymbol{\Phi}^{(1)}(u)$ denoting the composition on the manifold, we have $\boldsymbol{\Phi}^{(1)}(0) = \boldsymbol{\phi}^m$ and $\boldsymbol{\Phi}^{(1)}(1) = \boldsymbol{\phi}^e$.

The 1D manifold $\mathcal{M}_1$ is formed by the trajectory from the single point $\boldsymbol{\phi}^m$. The 2D manifold $\mathcal{M}_2$ is formed by the trajectories generated by all points on a curve $\mathcal{G}$, which is called the *manifold generator*. A specific choice of $\mathcal{G}$ is given below: here we itemize its basic required properties:

i) $\mathcal{G}$ is a simple closed curve in the realizable composition space, $\mathcal{C}_R$.

ii) $\mathcal{G}$ contains the mixing point $\boldsymbol{\phi}^m$.

iii) Coordinates of points on $\mathcal{G}$ are denoted by $\boldsymbol{\phi}^G(\theta)$, where the parameter θ takes values in the interval $[0, 2\pi]$.

It is convenient—and possible without imposing further requirements—to choose the parametrization so that

$$\boldsymbol{\phi}^G(0) = \boldsymbol{\phi}^G(2\pi) = \boldsymbol{\phi}^m. \tag{15}$$

Coordinates of points on the 2D manifold $\mathcal{M}_2$ are denoted by $\boldsymbol{\Phi}(r,\theta)$, where r and θ are the polar coordinates of points in the parameter space $\mathcal{P}$, which is the unit disk (see Fig. 1). For given θ, $\boldsymbol{\Phi}(r,\theta)$ is the trajectory generated by the point $\boldsymbol{\phi}^G(\theta)$ on the generator curve, with r being the normalized arclength, in this case measured from the equilibrium point, $\boldsymbol{\phi}^e$.

Thus in the parameter space $\mathcal{P}$ (Fig. 1) the origin ($r = 0$) corresponds to equilibrium ($\boldsymbol{\Phi}(0,\theta) = \boldsymbol{\phi}^e$); the unit circle ($r = 1$) corresponds to the generator curve ($\boldsymbol{\Phi}(1,\theta) = \boldsymbol{\phi}^G(\theta)$); and radial lines (constant θ) correspond to trajectories. The point $(r,\theta) = (1,0)$ corresponds to the mixing point ($\boldsymbol{\Phi}(1,0) = \boldsymbol{\phi}^m$), and the straight line segment between this point and the origin is the 1D manifold ($\boldsymbol{\Phi}^{(1)}(u) = \boldsymbol{\Phi}(1-u,0)$).

It remains to specify the manifold generator $\mathcal{G}$. If the kinetics are such that a 2D manifold method can be successful, then all trajectories rapidly approach a 2D attracting manifold (i.e. the intrinsic 2D manifold). To an extent, then, the choice of $\mathcal{G}$ may not be crucial: for, however $\mathcal{G}$ is chosen, the resulting manifold (except near $\mathcal{G}$ itself) will be close to the same attracting manifold. However, clearly $\mathcal{G}$ should be as "big" as possible, so as to maximize the overlap between $\mathcal{M}_2$ and the 2D intrinsic manifold.

Following the above arguments we now describe the specification of $\mathcal{G}$ which is based on the *extreme values* of *major species*. With there being n_e elements, the number of major species is specified to be $n_m = n_e + 2$. For the CO/H_2-air system ($n_e = 4$), a sensible choice of the major species is: CO, H_2, O_2, N_2, H_2O and CO_2. It is convenient to number the major species $1, 2, \ldots, n_m$, and then the remaining *minor species* are numbered $n_m + 1,\ n_m + 2, \ldots,\ n_s$.

The major species space $\mathcal{C}_M$, is the n_m-dimensional sub-space of $\mathcal{C}$ spanned by $\mathbf{e}_1, \mathbf{e}_2, \ldots, \mathbf{e}_{n_m}$. The realizable region in this space $\mathcal{C}_{MR}$ is the intersection of $\mathcal{C}_M$ and $\mathcal{C}_R$: it represents all realizable compositions in which the minor species are zero. The region $\mathcal{C}_{MR}$ is defined by n_e equality constraints from Eq. (5), $(n_s - n_m)$ equality constraints from the requirement that the minor species are zero, together with the inequalities $\phi_\alpha \geq 0$ (Eq. 4). Hence there are $n_s - 2$ equality constraints in total, so that $\mathcal{C}_{MR}$ is a two-dimensional convex polytope: its boundary $\partial\mathcal{C}_{MR}$ and its vertices correspond to extreme values of the major species.

For the CO/H_2-air mixture used in the examples, the curve $\partial\mathcal{C}_{MR}$ contains the mixing point $\boldsymbol{\phi}^m$, and hence satisfied all the requirements of the generator $\mathcal{G}$. For this case, we take $\partial\mathcal{C}_{MR}$ to be the generator $\mathcal{G}$.

In general, however, ϕ^m need not be contained in $\partial\mathcal{C}_{MR}$: for example, ϕ^m would not be in $\partial\mathcal{C}_{MR}$ if the unburnt mixture contained non-zero quantities of H_2O and CO_2. The above treatment is modified to handle the general case as now described and shown on Fig. 2.

For each fuel species (e.g. CO) there is an overall reaction (i.e. $CO + \frac{1}{2}O_2 \rightarrow CO_2$), and to each such reaction there is a corresponding reaction vector. The *overall reaction vector* $\mathbf{S}^0$ is defined as the sum of these reaction vectors, weighted with the specific mole number of the reactant in the mixture. This vector is used to divide the realizable major species region $\mathcal{C}_{MR}$ into two parts ($\mathcal{C}^+_{MR}$ and $\mathcal{C}^-_{MR}$) depending on whether the dot product $\mathbf{S}^0 \cdot (\phi - \phi^m)$ is non-negative, or negative, respectively. We then take the boundary of $\mathcal{C}^+_{MR}$, denoted by $\partial\mathcal{C}^+_{MR}$, to be the generator $\mathcal{G}$ (see Fig. 2).

For the CO/H_2-air system, the procedure described above was used to produce the 2D TGLDM. Figure 3 shows this 2D manifold in 13-space projected onto the $CO_2 - H_2O$ plane. The line around the perimeter is the generator $\mathcal{G}$, which contains the mixing point. The other solid lines are trajectories (i.e. $\boldsymbol{\Phi}(r,\theta), \theta$ =constant), which originate on $\mathcal{G}$ and terminate at equilibrium. It may clearly be seen that these trajectories converge on a 1D manifold, and then move along this manifold to ϕ_e. The bold line is the 1D TGLDM $\mathcal{M}_1$, i.e. the trajectory generated by ϕ_m.

The three dashed lines shown on Fig. 3, are $\boldsymbol{\Phi}(r,\theta)$ for the values $r = \frac{1}{4}, \frac{1}{2}$ and $\frac{3}{4}$. It may be seen that, in places, the constant r lines and the constant θ lines (i.e. trajectories) become aligned. This is a natural consequence of the bunching and convergence of trajectories, on which the method depends. But it indicates that the $r - \theta$ parametrization is ill-conditioned. For example, where the parameter lines become parallel, so do the tangent vectors $\partial\boldsymbol{\Phi}/\partial r$ and $\partial\boldsymbol{\Phi}/\partial\theta$. Then the denominator in Eq. (13) becomes zero.

It is necessary, then, to reparametrize the manifold to avoid this ill-conditioning. In the new parametrization chosen, the parameters u and v are the Cartesian coordinates of the unit square. Hence the singularity that occurs at $r = 0$ is also removed. (Space limitations do not permit a description of this reparametrization procedure.)

RESULTS: PERFECTLY-STIRRED REACTOR

For a simple test case corresponding to a perfectly stirred reactor (PSR), we now demonstrate the performance of the 1D and 2D TGLDM methods compared to detailed-kinetics calculations.

Using the full kinetics mechanism, the *transient* PSR calculations considered amount to the solution of the set of ordinary differential equations

$$\frac{d}{dt}\boldsymbol{\phi}(t) = \mathbf{S}(\boldsymbol{\phi}(t)) - (\boldsymbol{\phi}(t) - \boldsymbol{\phi}^m)\omega, \tag{16}$$

with the initial condition $\boldsymbol{\phi}(0) = \boldsymbol{\phi}^e$. Here ω is a specified rate, which is the inverse of the PSR residence time (i.e. $\omega = 1/\tau_{res}$). The term in ω is the perturbation $\mathbf{F}$ (see Eq. 8) that tends to move $\boldsymbol{\phi}(t)$ off the manifolds. For values of ω greater than the blow-out value $\omega_{\text{b.o.}}$, the long time solution to Eq. (6) is very close to $\boldsymbol{\phi}^m$, while for $\omega < \omega_{\text{b.o.}}$ it corresponds to stable (but incomplete) combustion. From the detailed kinetics solutions of Eq. (6) it is found that $\omega_{\text{b.o.}} \approx 1.53 \times 10^4 s^{-1}$ (i.e. $\tau_{\text{b.o.}} = 1/\omega_{\text{b.o.}} \approx 0.065ms$). For all the tests reported below we specify the value $\omega = 10^4 s^{-1} \approx 0.65\omega_{\text{b.o.}}(\tau_{\text{res}} = 0.1ms)$. This is a severe test of simplified schemes: for example, the temperature drops from its equilibrium value of 2,248K to a steady-state value of 1,459K.

Figure 4 shows the specific mole fractions of the major species O_2, H_2O and CO_2 against time. It may be seen that the 2D manifold method is in excellent agreement with the detailed scheme, and the agreement for the 1D method is also good—although there are discernible differences.

Figure 5 shows the corresponding results for H_2, which shows very interesting behavior. Just after $10^{-5}s$, there is an undulation in the detailed-scheme profile, which the 2D manifold method manages to follow, so that for large times the error in the 2D method is just a few percent. But the 1D manifold does not follow this behavior, and it underpredicts the asymptotic value by 35%. The results for the minor species are similar to those or H_2.

TRUNCATED PROJECTION

In the 2D manifold method, the evolution equations are solved for u and v, i.e. $\partial u/\partial t = \dot{u}_s + \dot{u}_F$, where $\dot{u}_s$ and $\dot{u}_F$ are the rates of change due to reaction

and the perturbation $\mathbf{F}$, respectively. In the implementation of the method, $\dot{u}_s$ is tabulated, and $\dot{u}_F$ is obtained from its defining equation: $\dot{u}_F = \mathbf{P}^u \cdot \mathbf{F}$. This involves the following operations: given u and v, $\mathbf{P}^u(u,v)$ and $\boldsymbol{\Phi}(u,v)$ are obtained by interpolation from the tables; $\mathbf{F}$ (which depends on $\boldsymbol{\phi}$) is determined; and then $\dot{u}_F$ is evaluated as $\mathbf{P}^u \cdot \mathbf{F}$. Both $\mathbf{P}^u$ and $\mathbf{F}$ are n_s-vectors, and hence if many species are involved (e.g. $n_s = 50$), the amount of computational work required by this evaluation is large. And the tabulation of the two n_s-vectors $\mathbf{P}^u(u,v)$ and $\mathbf{P}^v(u,v)$ requires considerable storage.

Motivated by these observations, we have developed a simplified approximate method for evaluating $\dot{u}_F$ and $\dot{v}_F$. It amounts to truncating the projection vectors $\mathbf{P}^u$ and $\mathbf{P}^v$in a particular basis.

In the n_s-dimensional composition space $\mathcal{C}$, consider a new set of orthonormal basis vectors $\tilde{\mathbf{e}}_\alpha$, obtained by a rotation of the $\mathbf{e}_\alpha$ axes. And let a tilde denote the components of any vector in this basis. Thus, in particular, we have $\boldsymbol{\phi} = \mathbf{e}_\alpha \phi_\alpha = \tilde{\mathbf{e}}_\alpha \tilde{\phi}_\alpha$, $\mathbf{F} = \mathbf{e}_\alpha F_\alpha = \tilde{\mathbf{e}}_\alpha \tilde{F}_\alpha$ and $\mathbf{P}^u = \mathbf{e}_\alpha P^u_\alpha = \tilde{\mathbf{e}}_\alpha \tilde{P}^u_\alpha$.

Now $\dot{u}_F$ is a scalar, and hence is the same in any Cartesian coordinate system: $\dot{u}_F = \mathbf{P}^u \cdot \mathbf{F} = P^u_\alpha F_\alpha = \tilde{P}^u_\alpha \tilde{F}_\alpha$.

The essential idea is to find a coordinate system (i.e. a choice of $\tilde{\mathbf{e}}_\alpha$) in which only the first few components of $\tilde{P}^u_\alpha$ are non-negligible. Then, if there are n_p of these non-negligible components, $\dot{u}_F$ can be approximated by

$$\dot{u}_F \approx \sum_{\alpha=1}^{n_p} \tilde{P}^u_{(\alpha)} \tilde{F}_{(\alpha)}. \tag{17}$$

Consequently, the computational work and storage required to evaluate $\dot{u}_F$ scale with n_p rather than with n_s.

There are certainly good reasons to suppose that such a coordinate system can be found. If the last n_e basis vectors $\tilde{\mathbf{e}}_\alpha$ ($\alpha = n_s - n_e,\ n_s - n_e + 1,\ \ldots, n_s$) are chosen to span the same subspace as the element vectors $\boldsymbol{\mu}_\beta$ (Eq. 2) then the last n_e elements of $\tilde{\mathbf{P}}^u$ are zero. And if, at a particular point on the manifold, $\tilde{\mathbf{e}}_1$ and $\tilde{\mathbf{e}}_2$ are chosen to span the same subspace as the tangent vectors $\boldsymbol{\Phi}_u$ and $\boldsymbol{\Phi}_v$ then (at that location) all but the first two components of $\tilde{\mathbf{P}}^u$ are zero.

The general method used to select the coordinate system is based on this last observation. We define the $n_s \times n_s$ matrix $T_{\alpha\beta}$ to be the area-average "covariance matrix" of the tangent vectors on the manifold. That is, with

angled brackets denoting an area average,

$$T_{\alpha\beta} = \langle \Phi'_{u\alpha} \Phi'_{u\beta} \rangle + \langle \Phi'_{v\alpha} \Phi'_{v\beta} \rangle, \tag{18}$$

where $\boldsymbol{\Phi}'_u = \boldsymbol{\Phi}_u - \langle \boldsymbol{\Phi}_u \rangle$. Then for each γ, the basis vector $\tilde{\mathbf{e}}_\gamma$ is chosen to be an eigenvector of $T_{\alpha\beta}$, corresponding to the γ-th largest eigenvalue. This procedure results in the average error (appropriately defined) in the approximation Eq. (17) to be minimized for each choice of n_p. The error is zero for $n_p \geq n_s - n_e$.

The efficacy of the truncated projection is clearly demonstrated in Fig. 6. This shows the 2D TGLDM calculation of H_2 (compared to the detailed scheme) for $n_p = 2, 3$ and 13. Clearly, the error incurred by truncating the projection is negligible for $n_p \geq 3$ and is not large for $n_p = 2$. Results for the other species support the same conclusions.

DISCUSSION

For convenience, the composition space $\mathcal{C}$ has been taken to be Euclidean. This implies a physical significance to the inner product in composition space—which cannot be justified on physical (or chemical) grounds. The inner product enters the development in two places: in the use of $\mathbf{S}^0 \cdot (\boldsymbol{\phi} - \boldsymbol{\phi}^m)$ to define the generator $\mathcal{G}$; and in taking $\mathbf{P}$ to be the perpendicular projection. On physical grounds, it is preferable to base $\mathbf{P}$ on the eigenvectors of $\partial S_\alpha(\boldsymbol{\phi})/\partial \phi_\beta$ (see Maas & Pope [9]). This removes the dependence of $\mathbf{P}$ on the inner product, but adds some complexity to the procedure. It is left to future work to determine how the choice of $\mathbf{P}$ affects the accuracy of the method.

In this paper we have considered 1D and 2D manifolds $\mathcal{M}_1$ and $\mathcal{M}_2$. (It is also consistent to define the zero-dimensional $\mathcal{M}_0$ manifold to be the equilibrium point $\boldsymbol{\phi}_e$.) The method can be extended to the general case of d dimensions ($1 \leq d \leq n_s - n_e$) as follows. The number of major species is specified to be $n_m = n_e + d$, so that the realizable region of the major-species space $\mathcal{C}_{MR}$ is d-dimensional. Its boundary $\partial\mathcal{C}_{MR}$ (or $\partial\mathcal{C}^+_{MR}$) then forms the $(d-1)$ generator $\mathcal{G}$ that generates the d-dimensional manifold $\mathcal{M}_d$. The hierarchy of manifolds thus defined ($\mathcal{M}_0$, $\mathcal{M}_1$, ..., $\mathcal{M}_{n_s-n_e}$) then has the property that $\mathcal{M}_{d-1}$ is contained in $\mathcal{M}_d$, and that the ultimate

manifold $\mathcal{M}_{n_s-n_e}$ consists of the whole realizable region $\mathcal{C}_R$, and at this level the method becomes exact.

For the premixed combustion considered here, there are (n_e+1) fixed thermochemical variables, namely the pressure p, the enthalpy h and (n_e-1) independent element mass fractions. In other situations, one or more of these quantities may vary in space or time. To take a specific example, in the simplified treatment of two-stream non-premixed combustion, all of these variables have a known linear dependence on the mixture fraction ξ. The TGLDM manifold method can be applied as described above, but with ξ being an additional parameter. Hence corresponding to the 2D manifold from premixed combustion, we obtain a 3D manifold for non-premixed combustion, with coordinates $\boldsymbol{\Phi}(u, v, \xi)$.

The present TGLDM method should be regarded as an alternative to—not a replacement for—the ILDM method. The advantages of TGLDM are: simplicity; that a natural parametrization is provided; and that a manifold of guaranteed simple topology is produced. On the other hand, the choice of the generator $\mathcal{G}$ requires the designation of certain species as "major", and may (close to $\mathcal{G}$) produce a manifold that is far from the optimum produced by the ILDM method. Future tests and experience with the methods will clarify and quantify their relative merits.

ACKNOWLEDGEMENT

This work was supported in part by Grant DE-FG02-90ER14128 from the U.S. Department of Energy, Chemical Sciences Division.

REFERENCES

1. Smooke, M.D., Mitchell, R.E., and Keyes, D.E., *Combust. Sci. Technol.* 67:85 (1989).

2. Warnatz, J., *Twenty-Fourth Symposium (International) on Combustion*, The Combustion Institute, Pittsburgh, 1992, p. 553.

3. Bilger, R.W., Ståner, S.H., and Kee, R.J., *Combust. Flame* 80:135 (1990).

4. Smooke, M.D., (Ed.), *Reduced Kinetic Mechanisms and Flames*, Springer, Berlin, 1992.

5. Peters, N., and Rogg, B. (Eds.), *Reduced Kinetic Mechanisms for Applications in Combustion Systems*, Springer, Berlin, 1993.

6. Keck, J.C., *Twenty-Second Symposium (International) on Combustion*, The Combustion Institute, Pittsburgh, 1989, p. 1705.

7. Chen, J.-Y., Combust. Sci., Technol. 57:89 (1988).

8. Frenklach, M., *Reduction of Chemical Reaction Models* in *Numerical Approaches to Combustion* (E.S. Oran and J.P. Boris, eds.) AIAA, Washington, DC, 1991, p. 129.

9. Maas, U. and Pope, S.B., *Combust. Flame* 88:239 (1992).

10. Maas, U. and Pope, S.B., *Twenty-Fourth Symposium (International) on Combustion*, The Combustion Institute, Pittsburgh, 1992, p. 103.

REFERENCES

1. Smooke, M.D., Mitchell, R.E., and Keyes, D.E., *Combust. Sci. Technol.* 67:85 (1989).

2. Warnatz, J., *Twenty-Fourth Symposium (International) on Combustion*, The Combustion Institute, Pittsburgh, 1992, p. 553.

3. Bilger, R.W., Ståner, S.H., and Kee, R.J., *Combust. Flame* 80:135 (1990).

4. Smooke, M.D., (Ed.), *Reduced Kinetic Mechanisms and Flames*, Springer, Berlin, 1992.

5. Peters, N., and Rogg, B. (Eds.), *Reduced Kinetic Mechanisms for Applications in Combustion Systems*, Springer, Berlin, 1993.

6. Keck, J.C., *Twenty-Second Symposium (International) on Combustion*, The Combustion Institute, Pittsburgh, 1989, p. 1705.

7. Chen, J.-Y., Combust. Sci., Technol. 57:89 (1988).

8. Frenklach, M., *Reduction of Chemical Reaction Models* in *Numerical Approaches to Combustion* (E.S. Oran and J.P. Boris, eds.) AIAA, Washington, DC, 1991, p. 129.

9. Maas, U. and Pope, S.B., *Combust. Flame* 88:239 (1992).

10. Maas, U. and Pope, S.B., *Twenty-Fourth Symposium (International) on Combustion*, The Combustion Institute, Pittsburgh, 1992, p. 103.

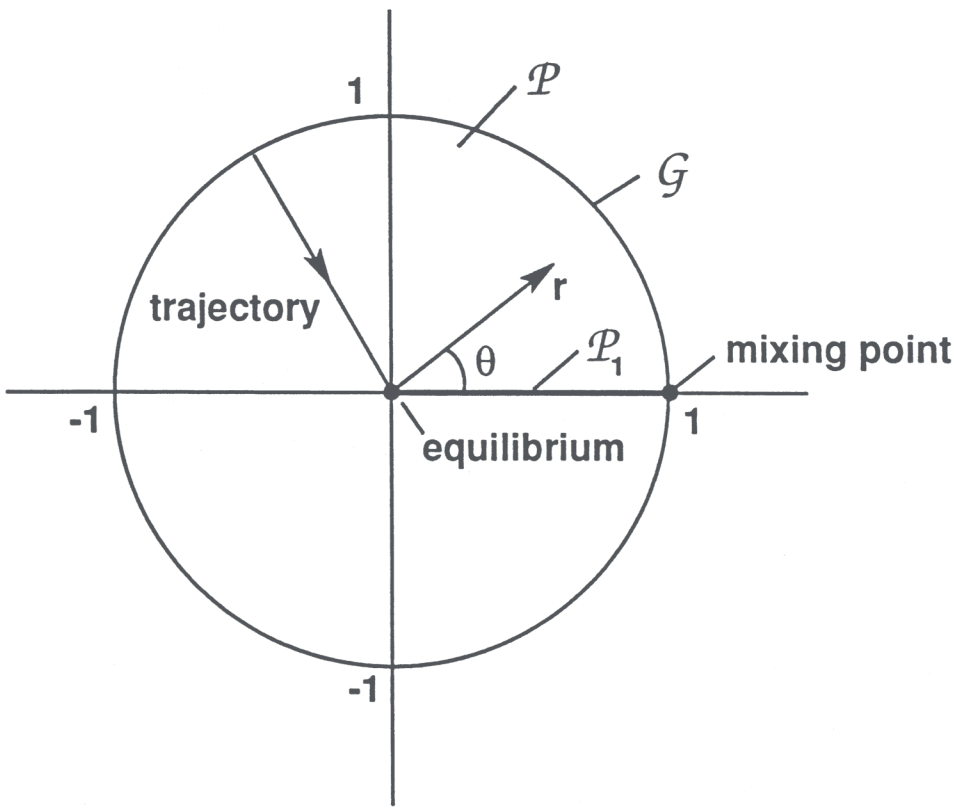

Fig. 1: Sketch of the parameter space $\mathcal{P}$ for the 2D TGLDM, $\mathcal{M}_2$, showing points corresponding to equilibrium, the mixing point, the generator $\mathcal{G}$, and a reaction trajectory. $\mathcal{P}_1$ is the parameter space for the 1D manifold $\mathcal{M}_1$.

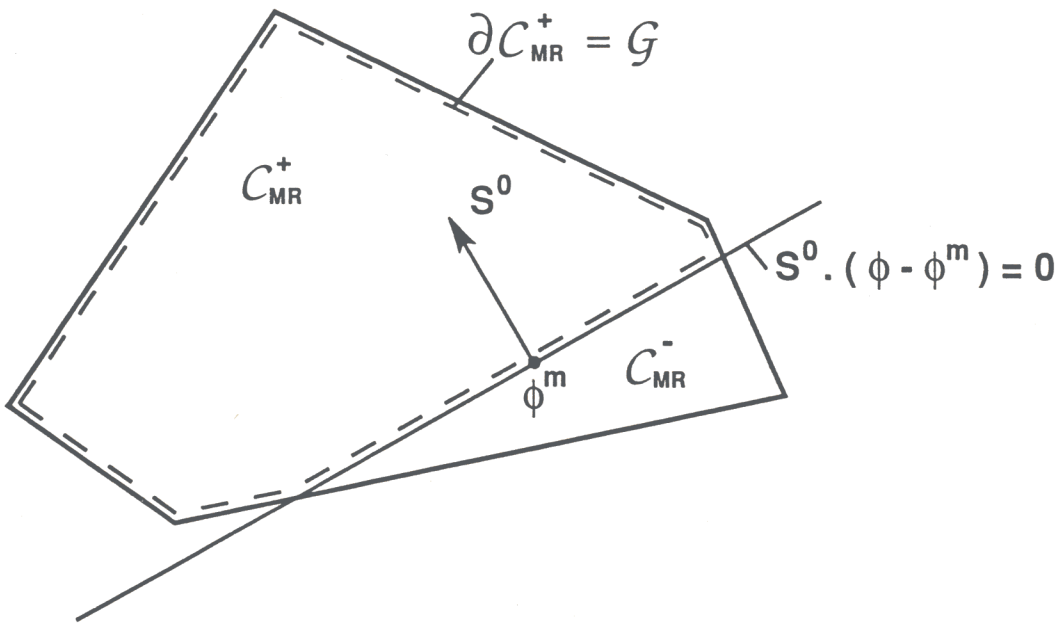

Fig. 2: Sketch of the major-species relizable region C_{MR}, showing the definition of the manifold generator $\mathcal{G}$.

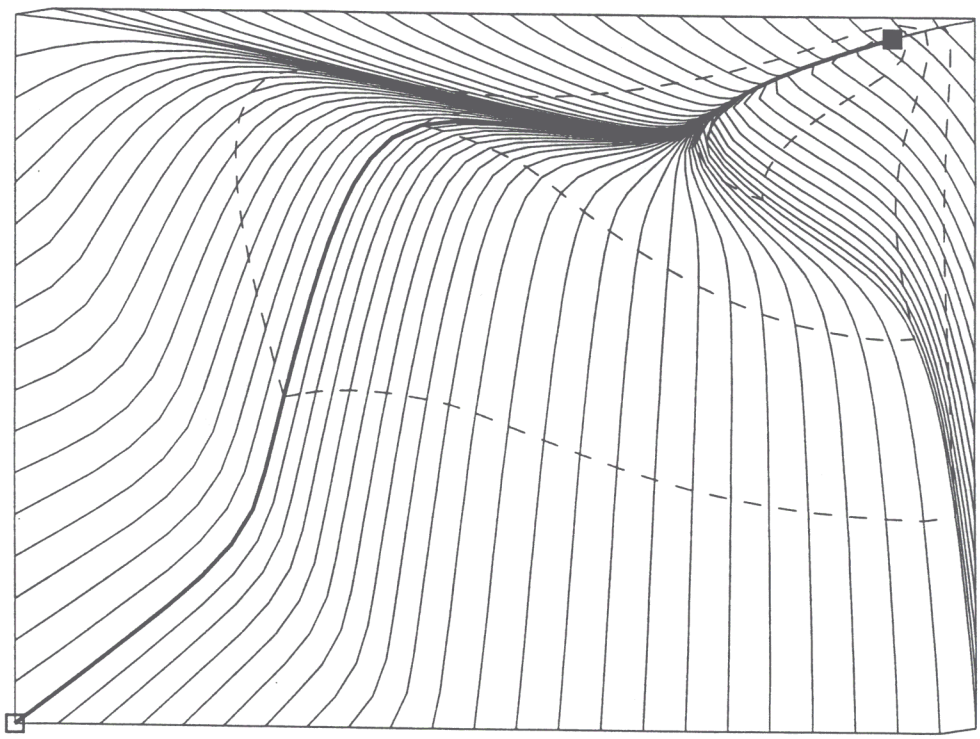

Fig. 3: The 2D TGLDM manifold $\mathcal{M}_2$ projected onto the $CO_2 - H_2O$ plane. Reaction trajectories go from the manifold generator $\mathcal{G}$ (the perimeter of the figure) to the equilibrium point (■). The 1D TGLDM manifold is the bold line from the mixing point (□) to equilibrium. The dashed lines are the projections of $\boldsymbol{\Phi}(r, \theta)$ for $r = \frac{1}{4}$, $\frac{1}{2}$ and $\frac{3}{4}$.

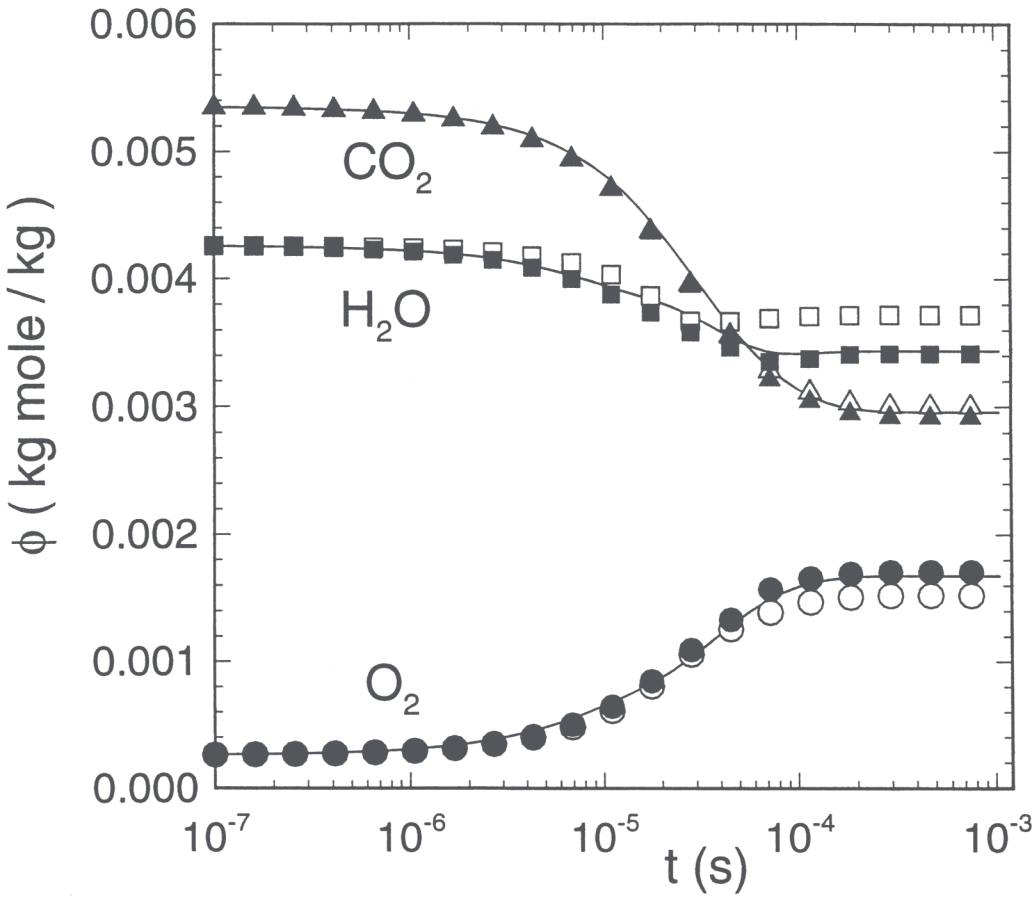

Fig. 4: Specific mole numbers of major species against time for the transient PSR test case, with $\omega = 10^4 s^{-1}$. Solid line, full kinetics; solid symbols, 2D TGLDM; open symbols, 1D TGLDM.

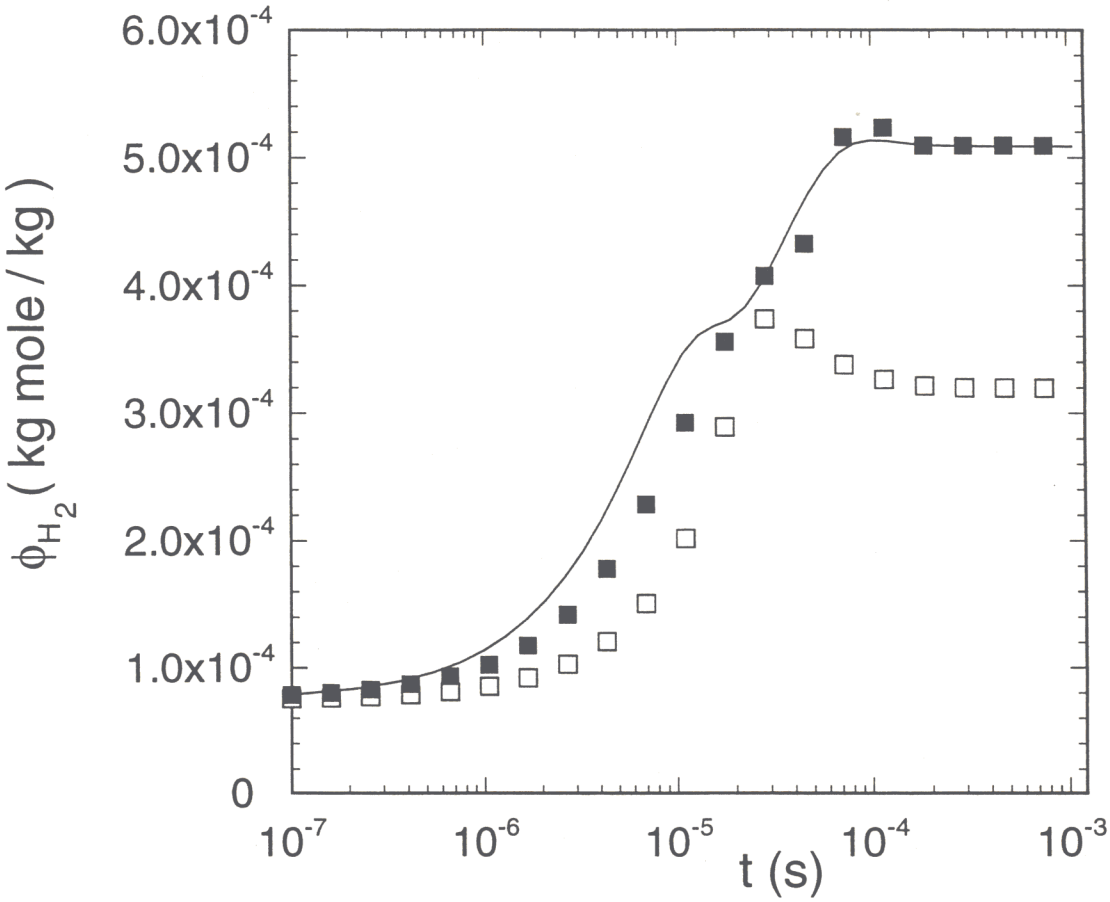

Fig. 5: Specific mole number of H_2 against time for the transient PSR test case, wth $\omega = 10^4 s^{-1}$. Solid line, full kinetics; solid symbols, 2D TGLDM; open symbols, 1D TGLDM.

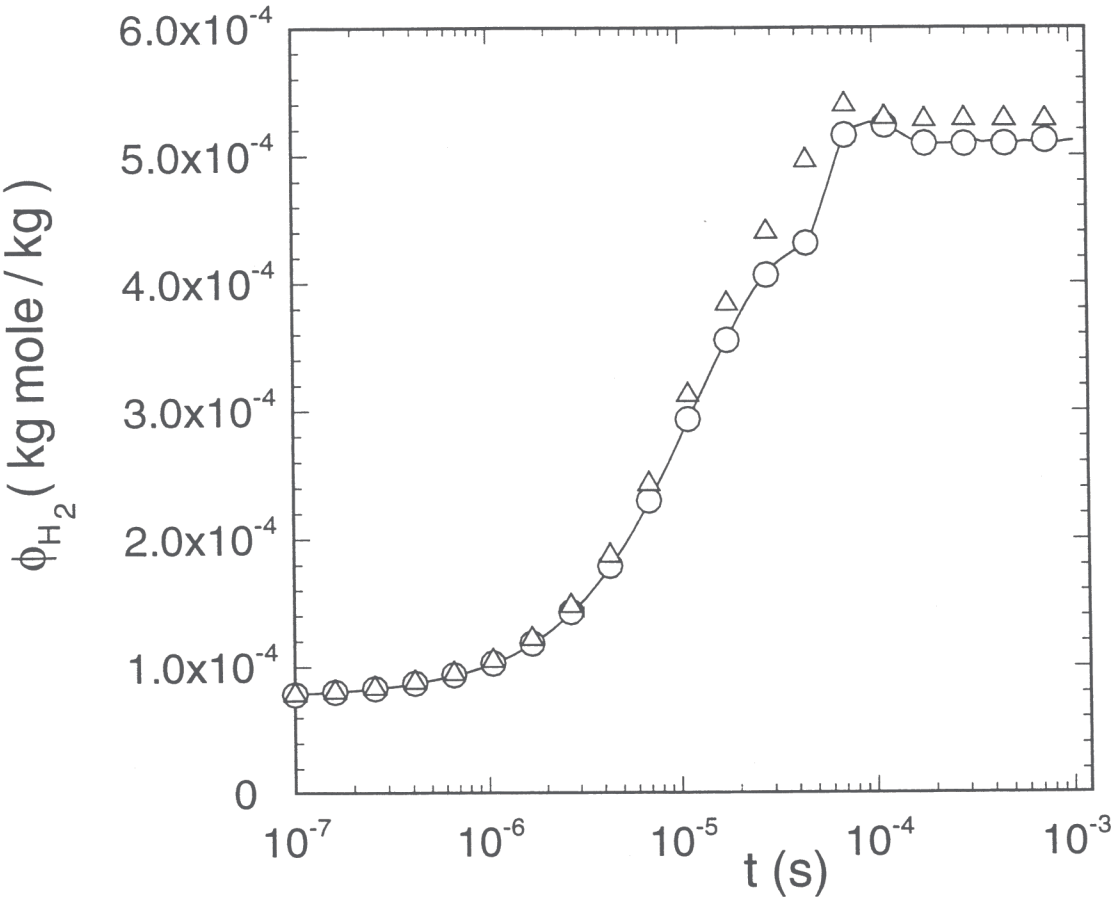

Fig. 6: Specific mole number of H_2 against time for the transient PSR test case, with $\omega = 10^4 s^{-1}$, for the 2D TGLDM with different truncations of the projection. Solid line, $n_p = 13$ (i.e. no truncation); triangles, $n_p = 2$; circles, $n_p = 3$.